Effect of anionic ordering on the electronic and optical properties of $BaTaO_2N$: TB-mBJ density functional calculation

K Bettine[1], O Sahnoun[1], M Sahnoun[1,†], and M Driz[2]

[1] *LPQ3M, University Mustapha Stambouli of Mascara, Algeria*
[2] *University Djilali Liabes of Sidi Bel Abbes, Algeria*

(Received 1 November 2016; revised manuscript received 15 February 2017; published online 30 March 2017)

This report presents a first-principles investigation of the structural, electronic, and optical properties of perovskite oxynitrides $BaTaO_2N$ by means of density functional theory (DFT) calculations using the full-potential linearized augmented plane wave (FP-LAPW) method. Three possible structures (*P*4*mm*, *I*4/*mmm*, and *Pmma*) are considered according to the TaO_4N_2 octahedral configurations. The calculated structural parameters are found to be in good agreement with the previous theoretical and experimental results. Moreover, the electronic band structure dispersion, total, and partial densities of electron states are investigated to explain the origin of bandgaps and the contribution of each orbital's species in the valence and the conduction bands. The calculated minimum bandgaps of the *P*4*mm*, *I*4/*mmm*, and *Pmma* structures are 1.83 eV, 1.59 eV, and 1.49 eV, respectively. Furthermore, the optical properties represented by the dielectric functions calculated for $BaTaO_2N$ show that the *I*4/*mmm* phase absorbs the light at a large window in both the visible and UV regions, whereas the other two structures (*P*4*mm* and *Pmma*) are more active in the UV region. Our investigations provide important information for the potential application of this material.

Keywords: first-principles calculations, perovskite oxynitrides, electronic properties, optical properties

PACS: 71.15.Mb, 71.20.Nr, 74.25.Gz, 74.62.En **DOI:** 10.1088/1674-1056/26/5/057101

1. Introduction

Recently, perovskite oxynitrides have received considerable attention due to their appropriate properties such as a high dielectric constant,[1] visible light absorption,[2] photocatalytic activity,[3,4] photoelectrodes for water splitting,[5–8] colossal magneto-resistance,[9] and nontoxic colored pigment materials.[2] The perovskite oxynitrides with the chemical formula ABO_2N can frequently be described as derivatives of oxides ABO_3, formed by simultaneous substitutions of cation and anion components.[1] However, the perovskite oxynitrides prove to have valuable properties compared to the perovskite oxides. Thus, these features originate from the simultaneous interaction between oxygen and nitrogen ions, which have different polarizability, electronegativity, coordination numbers, and ionic radii.[10] Therefore, one possible way to change the properties of these materials and adjust them to specific applications is varying the O/N ratio or/and the ordering anions in the structures. In the perovskite oxynitrides ABO_2N, each *B* cation is surrounded by four O and two N ions, there are then two possible anion configurations: the two N ions can occupy either adjacent sites (cis-type) with 90° N–Ta–N in the octahedron TaO_4N_2 or opposite sites (trans-type) with 180° N–Ta–N in the octahedron TaO_4N_2. These distributions have pronounced effects on the physical properties, particularly the dielectric and optical properties.[11–13] Consequently, considerable efforts have been made to synthesize oxynitrides with ordered anions.[14–16]

The perovskite oxynitride $BaTaO_2N$ was first synthesized by Marchand *et al.*[17] Its dielectric property was found to be quite remarkable.[1] The compound is very stable in air, water, and acids, and contains relatively nontoxic elements.[11] The neutron diffraction studies reported a cubic structure with $Pm\bar{3}m$ symmetry, and a random O/N distribution in $BaTaO_2N$.[18] The density functional theory (DFT) studies have adopted also a random distribution of oxygen and nitrogen atoms with lower symmetry due to the local distortions of the bonds between oxygen and nitrogen.[19] Also, it was found that the cis-type distribution is preferred energetically over the trans-type distribution.[19] These results were supported by x-ray,[11] electron, and neutron diffraction measurements.[1] The latter has found that there is no anion order on a long-range in $BaTaO_2N$, while on a local scale the TaO_4N_2 octahedral principally approves a cis-type.[11]

The purpose of this paper is to investigate the effect of the TaO_4N_2 octahedral configurations on the structural, electronic, and optical properties from the cubic structure parent $BaTaO_2N$, using the density functional theory (DFT) within the generalized gradient approximation of Perdew–Burke–Ernzerhof for solids (PBEsol)[20] and that of the Tran–Blaha modified Becke–Johnson (TB-mBJ),[21] thus to better understand the behavior of the perovskite oxynitrides and to validate several theoretical and experimental results. The overall structure of the paper is as follows. Specific calculation details are given in Section 2. Section 3 presents the results for structural and electronic properties, and the effective mass of the $BaTaO_2N$ structures. These results allow us to proceed with

†Corresponding author. E-mail: sahnoun_cum@yahoo.fr

© 2017 Chinese Physical Society and IOP Publishing Ltd

the analysis of their optical properties (Section 4). Finally, a summary of our results is given in Section 5.

2. Details of calculation

We have performed the calculations for three phases of $BaTaO_2N$ (*P*4*mm*, *I*4/*mmm*, and *Pmma*), using the full-potential linearized augmented plane-wave (FP-LAPW) method in its density functional theory formalism as implemented in the WIEN2k code.[22] In this method, the basis set is obtained by dividing the unit cell into non-overlapping spheres and an interstitial region. We have used two forms of approximation, namely, the PBEsol[20] and the TB-mBJ,[21] to describe the exchange–correlation potential. The values of $R_{MT}K_{max} = 7.0$ and $l_{max} = 10$ are kept throughout all the calculations. The Monkhorst–Pack denser *k*-meshes ($27 \times 27 \times 27$) are used for the three structures, since we have found that our results are very sensitive to the *k*-mesh. The muffin-tin radii are taken as (2.5, 1.96, 1.69, 1.64) a.u. for (Ba, Ta, O, N), respectively. The calculations are iterated until the total energies are converged below 10^{-5} Ry. The calculations are performed with relaxation of both atomic positions and cell parameters. The TB-mBJ potential approximation approach is considered to be better than the PBEsol for the calculation of bandgaps.[21,23–25] Consequently, we have calculated the electronic and optical properties using the TB-mBJ approach.

3. Results and discussion

3.1. Structural properties

The perovskite oxynitride $BaTaO_2N$ has a cubic structure $Pm\bar{3}m$ with a disorder of the nitrogen and oxygen atoms.[18] After ordering, the cubic structure changes to the tetragonal structure with two different space groups *P*4*mm* (trans-type) and *I*4/*mmm* (trans-type), and to the orthorhombic structure with space group *Pmma* (cis-type) according to the TaO_4N_2 octahedral configurations in the structure. The minimum total energy of the unit cell for a number of different volumes of $BaTaO_2N$ structure has been calculated. We have checked the structure stability by studying the *P*4*mm*, *I*4/*mmm*, and *Pmma* crystals through the fit to the Murnaghans equation of state (EOS) of the total energy versus volume.[26] The c/a and b/a ratios have also been optimized for each crystal volume. As shown in Fig. 2, the *Pmma* structure is more stable than the *P*4*mm* and *I*4/*mmm* structures.

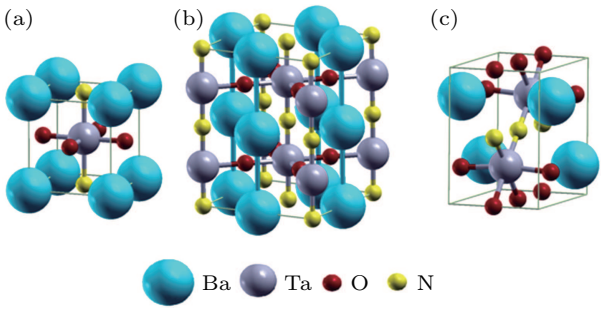


Fig. 1. (color online) Unit cell of the three structures of $BaTaO_2N$: (a) *P*4*mm* (polar-trans), (b) *I*4/*mmm* (non-polar-trans), and (c) *Pmma* (antipolar-cis).

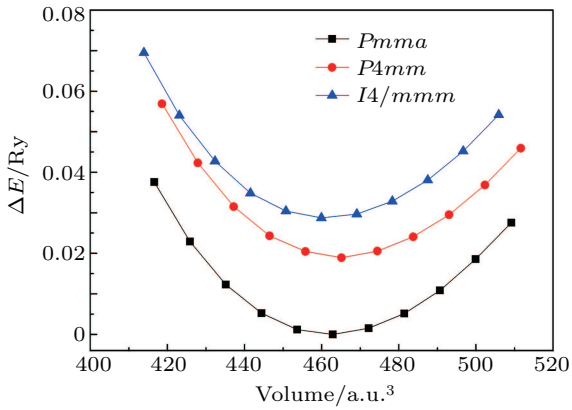


Fig. 2. (color online) Relative total energy differences calculated for the three structures of $BaTaO_2N$: (a) *P*4*mm* (polar-trans), (b) *I*4/*mmm* (non-polar-trans), and (c) *Pmma* (antipolar-cis). The lowest total energy is set to 0 Ry.

Table 1. Calculated lattice parameters, bulk moduli B_0, and interatomic distances for the three structures of $BaTaO_2N$ at zero pressure along with available experimental and theoretical data.

Structure	*P*4*mm*			*I*4/*mmm*		*Pmma*	
	Cal.	Theo.	Exp.	Cal.	Exp.	Cal.	Exp.
a/Å	4.06	4.06[19]	4.10[11]	5.78	5.81[11]	5.78	5.79[11]
b/Å						4.06	4.14[11]
c/Å	4.19	4.22[19]	4.13[11]	8.19	8.23[11]	5.82	5.79[11]
V/Å^3	69.07			68.05		68.30	
B_0/GPa	199			203		202	
Ba–O/Å	(4x)2.8651			(8x)2.8923		(4x)2.8601	
	(4x)2.9713					(1x)2.8040	
						(2x)2.8988	
						(1x)3.0141	
Ba–N/Å	(4x)2.8751			(4x)2.8880		(4x)2.9165	
Ta–O/Å	(4x)2.0347			(4x)2.0422		(2x)2.1291	
						(2x)2.0365	
Ta–N/Å	(1x)1.9479			(1x)2.0479		(2x)1.9804	
	(1x)2.2407			(1x)2.0483			

We have confirmed our results in the stable *Pmma* structure by comparison with other theoretical[27] and experimental data.[11] It is clear that our calculated lattice parameters for the *P*4*mm*, *I*4/*mmm*, and *Pmma* structures agree very well with the experiment ones.[11] The bulk moduli of the three structures are very close to each other. Table 1 summarizes the equilibrium lattice parameters and bulk moduli *B* for the studied structures. The atomic positions are listed in Table 2. The calculations show that the space group of $BaTaO_2N$ strongly depends on the distribution of oxygen and nitrogen in the octahedron TaO_4N_2. The bond lengths and the atomic arrangements around Ta and Ba sites are also summarized in Tables 1 and 2 and shown in Fig. 1, respectively.

Table 2. Atomic coordinates for the three structures of $BaTaO_2N$.

Structure	Atom	Site	*X*	*Y*	*Z*
*P*4*mm* (trans)	Ba	1(a)	0.0	0.0	0.0
	Ta	1(b)	0.5	0.5	0.4907
	O	2(c)	0.5	0.0	0.5177
	N	1(b)	0.5	0.5	0.0257
*I*4/*mmm* (trans)	Ba	4(c)	0.5	0.0	0.5
	Ta	4(e)	0.5	0.5	0.2499
	O	8(f)	0.75	0.75	0.25
	N(1)	2(a)	0.5	0.5	0.0
	N(2)	2(b)	0.0	0.0	0.0
Pmma (cis)	Ba	2(e)	0.25	0.0	0.2404
	Ta	2(f)	0.75	0.5	0.2680
	O(1)	2(b)	0.5	0.5	0.0
	O(2)	2(e)	0.75	0.0	0.2416
	N	2(d)	0.5	0.5	0.5

The Ta–O/N distance indicates the asymmetric coordination around Ta, which implies various octahedral configurations with different energies in the *P*4*mm* and *Pmma* structures. For the *P*4*mm* structure, the Ta–N bond length has two different values, and the Ta–O bond length is comprised in between these two values. However, the *I*4/*mmm* structure presents a slight ocahedron TaO_4N_2 distortion corresponding to almost the same Ta–O and Ta–N bond lengths with a difference of 0.6%. While, in the *Pmma* structure, the two Ta–N similar bond lengths are 15% different compared to the two Ta–O bond lengths, which is more significant than the other structures.

3.2. Electronic properties

The physical properties of many compounds are correlated to their electronic band structures, while the basis of the band structure can be related to the density of state. In this section, we present the electronic properties of the three polymorphs of $BaTaO_2N$. As we can see, there is an important influence of the ordering anions (O/N) on the electronic structure, especially on the energy gap of $BaTaO_2N$. The electronic band structures at equilibrium volume are shown in Fig. 3, which are drawn along the symmetry directions in the first Brillouin zone (Fig. 4). The zero of the energy is set at the top of the valence band. The valence band (VB) and the conduction band (CB) states for the *I*4/*mmm* and *Pmma* structures are more dispersive compared to that of the *P*4*mm* structure. They indicate that hybridization interactions play an important role in chemical bonding of the *I*4/*mmm* and *Pmma* structures. The results (see Fig. 3) clearly show that the *P*4*mm* (polar-trans) structure is a semiconductor with an indirect bandgap. The valence band maxima (VBM) locate at *M* and *A* points, while the conduction band minimum (CBM) locates at the Γ point. While the other two structures are semiconductors with direct band gaps at the Γ point. It is interesting to observe that the effective electronic bandgap, found in the vicinity of the *P*4*mm* (polar-trans) structure, is around 1.838 eV, which is larger than that of the *I*4/*mmm* (non-polar-trans) structure, 1.587 eV. It is also larger than that of the *Pmma* (antipolar-cis) structure, 1.496 eV. Our calculated energy bandgaps are approaching to the experimental value (1.8 eV).[1] The relaxation of atomic positions leads to an asymmetry in the Ta–N bond lengths (1.8945 Å/2.2885 Å) in the *P*4*mm* (polar-trans) structure; their minimum is slightly shorter than that in the *I*4/*mmm* (non-polar-trans) structure (2.0479 Å). The differences in the atomic arrangements and Ta–N bond lengths lead to different bandgaps. Accordingly, as a consequence to the polarity trend, the bandgap is influenced by the internal electric fields (polar vs. non-polar-trans-type orderings), which creates in a polar structure an asymmetry in the Ta–N bond lengths. The non-polar structure has no internal electric field; there is no noticeable difference between Ta–N bond lengths. As the bonds become more polar, the greater the energy gained upon transferring electrons between atoms, the wider the bandgap compared to the non-polar structure. There is also another unfavorable consequence to the polarity trend. An important feature of the electron band structure is the curvature of the bands at zone center, which is inversely proportional to the electron and hole effective masses. The lower the bandgap, the greater the repulsion between the conduction and valence bands, and the higher the curvature away from the zone center. It is also significant to note that the bandgap is not influenced by the orientation of TaO_4N_2 octahedra (non-polar-trans-type vs. antipolar-cis-type orderings); their Ta–N bond lengths are symmetric and have almost the same values.

To investigate the origin of the states in the band structure of $BaTaO_2N$, the total densities of states (TDOS) have been studied. The TDOS for the three phases are quite similar. Figure 5 presents the TDOS for *P*4*mm*, *I*4/*mmm*, and *Pmma* structures. In this figure, the lowest valence bands are split into two sharp subbands and are located in the energy range from −13.9 eV to −10.1 eV for the *P*4*mm* structure, from −14.24 eV to −10.1 eV for the *I*4/*mmm* structure, and from −14.6 eV to -10.6 eV for the *Pmma* structure. These bands originate from the Ba-5p and N-2s states. The upper valence bands between around −6.42 eV and 0 eV for the *P*4*mm* structure and between around −6.9 eV and 0 eV for

the $I4/mmm$ and *Pmma* structures consist mainly of O-2p and N-2p states, which are strongly hybridized with Ta-5d states for all structures. The strong hybridization leads to further covalent bonding and a less ionic character. We can note that the *Pmma* structure has two types of nitrogen atoms, N(1) and N(2), where the contribution of the N(2) atoms in the upper valence bands is more important than that of the N(1) atoms. Also, the width of the upper valence bands of the cis-type configuration (*Pmma*) is larger than that of the trans-type configuration (*P*4*mm* and $I4/mmm$), which depends on the ordering of nitrogen atoms in the structure. The upper part of the valence band is dominated by N-2p states, while O-2p states are mainly in the lower part in both trans-type structures, however, there is a mixing between N-2p and O-2p states in the valence band for the cis-type structure, a consequence of the lowered symmetry of the TaO_4N_2 octahedra. The lower conduction band above 6 eV is dominated by Ta-5d, associated with a small contribution from O-2p, N-2p, and Ba-5d states.

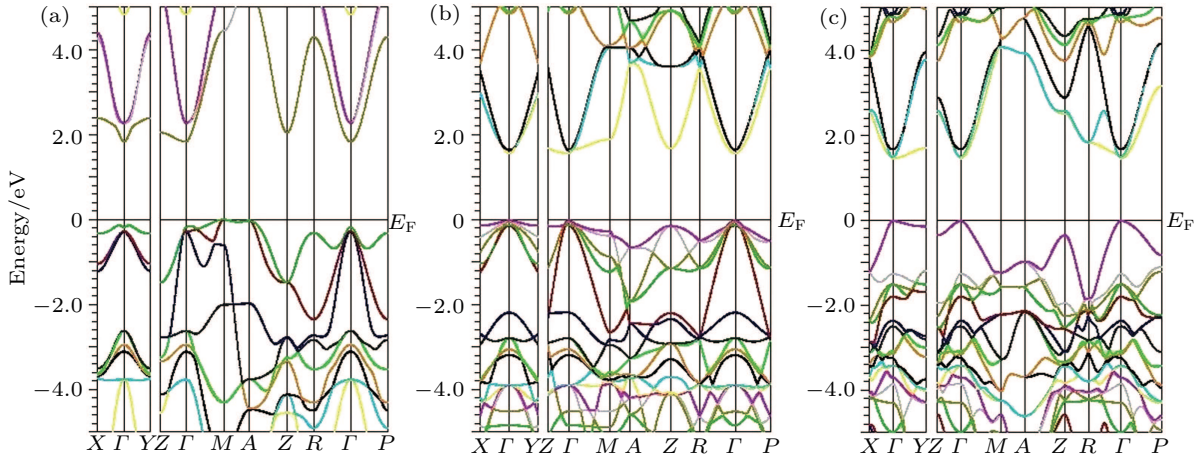


Fig. 3. (color online) The electronic band structures along the high symmetry points for the three structures of $BaTaO_2N$: (a) *P*4*mm* (polar-trans), (b) $I4/mmm$ (non-polar-trans), and (c) *Pmma* (antipolar-cis).

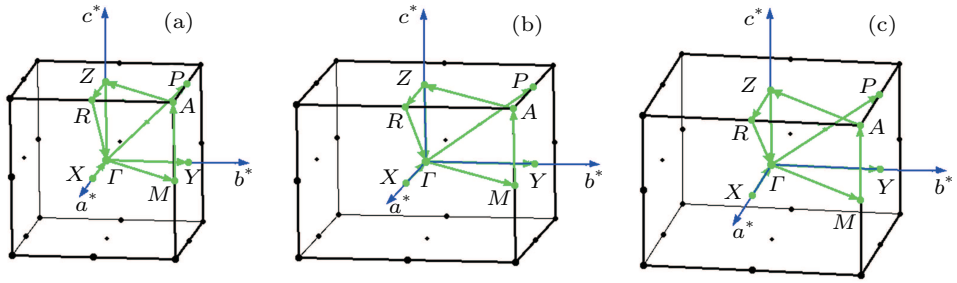


Fig. 4. (color online) Selected directions in the primitive Brillouin zone for the three structures of $BaTaO_2N$: (a) *P*4*mm* (polar-trans), (b) $I4/mmm$ (non-polar-trans), and (c) *Pmma* (antipolar-cis).

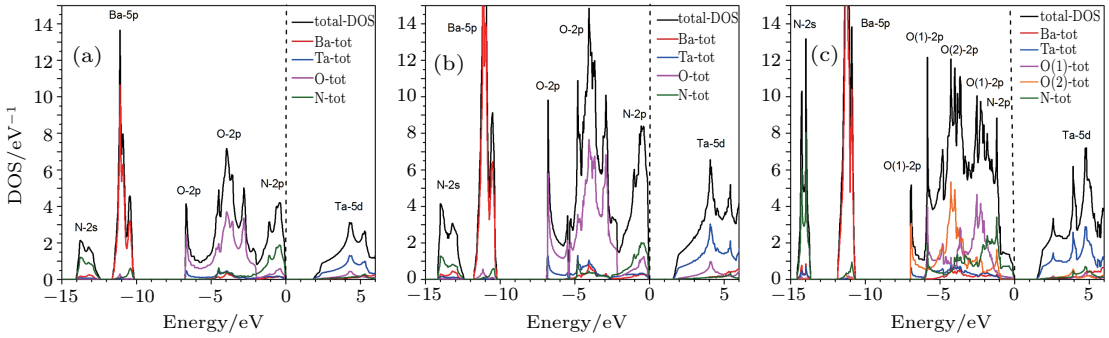


Fig. 5. (color online) The densities of state for the three structures of $BaTaO_2N$: (a) *P*4*mm* (polar-trans), (b) $I4/mmm$ (non-polar-trans), and (c) *Pmma* (antipolar-cis).

3.3. Effective mass

The most significant description of the energy offered to electrons is generally simplified by considering the variations of the energy E as a function of the wave vectors k along the directions of the highest symmetry in the reciprocal space. The conduction and valence bands are multiple, but the electronic transport properties depend mainly on the structure of the lowest conduction band and that of the highest valence band. In

our three structures, the conduction band presents a curvature that is very accentuated in the vicinity of its minimum Γ. Theoretically, the electron effective mass is determined by fitting the electronic conduction band structure to a parabolic model function in the first Brillouin zone. The electron effective mass m^* is then calculated in the conduction band along $\Gamma \rightarrow Y$, $\Gamma \rightarrow Z$, and $\Gamma \rightarrow R$ directions for the three structures in the k space using the following well-known relation:

$$\frac{1}{m^*} = \frac{1}{\hbar}\frac{\partial^2 E(k)}{\partial k^2}. \tag{1}$$

According to the Drude model, the mobility can be defined as qt/m^*, where q is the elementary charge, t is the relaxation time, and m^* is the effective mass. From the band structure, a degeneracy is observed in the bottom of the conduction band at the Γ point in the Brillouin zone for the $I4/mmm$ and *Pmma* structures, however this characteristic is not observed for the *P*4*mm* structure. There is also the presence of many different valleys on the conduction band, not far to the center Γ point of the Brillouin zone. The valleys characterized by low curvature correspond to electrons with high effective mass and consequently low electronic mobility. The calculated electron effective masses of the three structures are presented in Table 3.

Table 3. Calculated bandgaps and effective mass for the three structures of $BaTaO_2N$.

Structure	Bandgap/eV				Effective mass		
	Cal.		Theo.	Exp.	m^*/m_e		
	$\Gamma \rightarrow \Gamma$	$M \rightarrow \Gamma$			$\Gamma \rightarrow Y$	$\Gamma \rightarrow Z$	$\Gamma \rightarrow R$
*P*4*mm* (polar-trans)	2.01	1.83		1.8[1]	0.012	0.116	0.015
$I4/mmm$ (non-polar-trans)	1.59		1.3[27]		0.007	0.083	0.008
Pmma (anti-polar-cis)	1.49		1.6[27]		0.080	0.018	0.915

4. Optical properties

Since the optical properties and the electronic properties are correlated in solid materials, the frequency dependent dielectric function can be calculated from the energy band structure and has significant consequences on the physical properties of the material. The imaginary part $\varepsilon_2(\omega)$ of the complex dielectric tensor is calculated from the momentum matrix element between occupied and unoccupied wave functions, corresponding to the inter-band transitions. The imaginary part is given as

$$\varepsilon_2(\omega) = \frac{4\pi^2 e^2}{Vm^2\omega^2} \times \sum_{nn'\sigma} \langle kn\sigma|p|kn'\sigma\rangle\langle kn'\sigma|p|kn\sigma\rangle \times f_{kn}(1-f_{kn'})\delta(E_{kn'}-E_{kn}-\hbar\omega), \tag{2}$$

where m and e are the mass and the charge of electron, respectively, ω is the angular frequency of the electromagnetic radiation, V is the unit cell volume, p corresponds to the momentum operator, $|kn\sigma\rangle$ is the wave function of the crystal with the crystal momentum (wave vector) k, and σ is the spin corresponding to energy eigenvalue E_{kn}. Fermi distribution function f_{kn} makes a certain count of transitions from the occupied to unoccupied states. The term $\delta(E_{kn'}-E_{kn}-\hbar\omega)$ indicates a condition for the conservation of total energy, resulting in the summation of the combined density of states. The real part of the dielectric function, $\varepsilon_1(\omega)$, is calculated from the imaginary part of the dielectric function using the Kramer–Krœning relation

$$\varepsilon_1(\omega) = 1 + \frac{2}{\pi}\mathrm{P}\int_0^\infty \frac{\omega'\varepsilon_2(\omega')}{\omega'^2-\omega^2}\,\mathrm{d}\omega'. \tag{3}$$

The complex dielectric function is then given as

$$\varepsilon(\omega) = \varepsilon_1(\omega) + \mathrm{i}\varepsilon_2(\omega). \tag{4}$$

In order to show the influence of the distribution of nitrogen on the optical properties of $BaTaO_2N$, the dielectric function $\varepsilon(\omega)$ is calculated for the *P*4*mm*, $I4/mmm$, and *Pmma* structures of $BaTaO_2N$. The real part $\varepsilon_1(\omega)$ and the imaginary part $\varepsilon_2(\omega)$ of the calculated dielectric function are shown in Figs. 6 and 7, respectively. The dielectric function spectra (Figs. 6 and 7) show that the $I4/mmm$ phase noticeably absorbs the light at a large window in both the visible and UV regions, whereas the other two structures (*P*4*mm* and *Pmma*) are more active in the UV region. It is noted that for the *P*4*mm* and $I4/mmm$ structures, ε^{xx} and ε^{yy} are isotropic with the same value, while ε^{zz} reveals an anisotropic behavior. However, there is a considerable anisotropy between the three components for the *Pmma* structures. There are almost two main peaks located at the same region around 3.5 eV and 4.8 eV, with a slight shift, in all the three structures, whereas a strong absorption peak at 2.85 eV in the visible region is created only for the $I4/mmm$ structure. Only peaks with higher intensities are considered. The transition between the anions 2p states of the valence band (VB) to the unoccupied Ta-5d state in the conduction band mainly contributes to the peaks in the imaginary part $\varepsilon_2(\omega)$. The real part of the dielectric function $\varepsilon_1(\omega)$ is also displayed in Fig. 6. This function $\varepsilon_1(\omega)$ gives us information about the electronic polarizability of a material. As materials behave as metallic for negative values of $\varepsilon_1(\omega)$ and are dielectric otherwise,[28,29] $BaTaO_2N$ is metallic at 4.86 eV and 5.31 eV in both trans configurations of *P*4*mm* and $I4/mmm$, respectively.

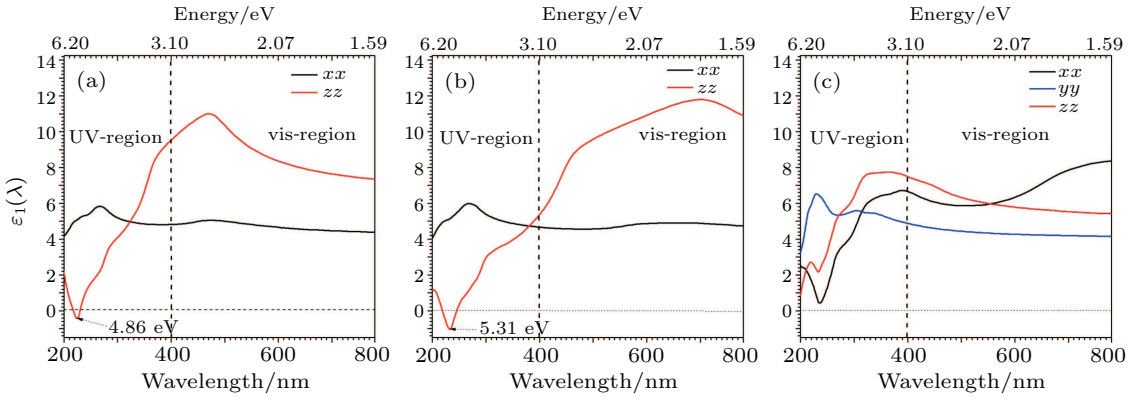


Fig. 6. (color online) The real part $\varepsilon_1(\omega)$ of the dielectric function for the three structures of $BaTaO_2N$: (a) *P*4*mm* (polar-trans), (b) *I*4/*mmm* (non-polar-trans), and (c) *Pmma* (antipolar-cis).

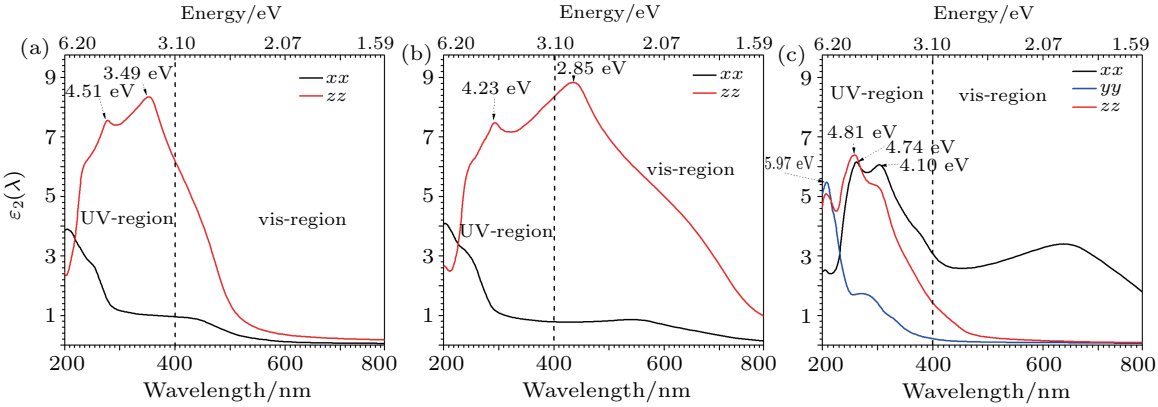


Fig. 7. (color online) The imaginary part $\varepsilon_2(\omega)$ of the dielectric function for the three structures of $BaTaO_2N$: (a) *P*4*mm* (polar-trans), (b) *I*4/*mmm* (non-polar-trans), and (c) *Pmma* (antipolar-cis).

5. Conclusion

The paper reports on the theoretical investigation of anionic ordering and electronic structures of $BaTaO_2N$ using the first-principles density-functional theory. The approximation (GGA-PBEsol) was used to calculate the structural properties, while the approximation (TB-mBJ) was used to study the band structure and density of states, which give clear details about the orbitals involved in the band formation. Comparing three different structures of the $BaTaO_2N$ compound, two aspects have been in focus: the influence of the internal electric fields (comparison of polar and non-polar-trans-type orderings) and the dependence on geometry (comparison of trans- and cis-oriented TaO_4N_2 octahedra). The present results indicate that the electronic and optical properties are strongly related with the TaO_4N_2 octahedral configurations. The bandgap is influenced by the internal electric fields (polar vs. non-polar-trans-type orderings), which creates an asymmetry in the Ta–N bond lengths. Although, it is not influenced by the orientation of TaO_4N_2 octahedra (non-polar-trans-type vs. antipolar cis-type orderings), their Ta–N bond lengths are symmetric and have almost the same values. The hybridization between anion 2p and Ta-5d states are responsible for the covalent bond between Ta–N and Ta–O. As a consequence, the valence band dispersion increases and pushes the top of the valence band towards the Fermi level. Moreover, the electron effective mass m^* was also calculated in the first Brillouin zone. The real and imaginary parts of the dielectric function were calculated. The peaks in the calculated spectra of $\varepsilon_2(\omega)$ show transitions of electrons from occupied bands to unoccupied bands. As a result, the $BaTaO_2N$ is a better suited material for potential application as a light absorber in a solar energy conversion device, optoelectronic devices, and photoelectrochemical water splitting under visible light.

Acknowledgement

The computational resources and services used in this work were provided by the HPC-Emir (High Performance Computing HPC), funded by Mascara University.

References

[1] Kim I M, Woodward P M, Baba-Kishi K Z and Tai C W 2004 *Chem. Mater.* **16** 1267
[2] Jansen M and Letschert H 2000 *Nature* **404** 980
[3] Kasahara A, Nukumizu K, Takata T, Kondo J N, Hara M, Kobayashi H and Domen K J 2003 *Phys. Chem. B* **107** 791
[4] Sato S and White J M 1980 *Chem. Phys. Lett.* **72** 83
[5] Lewis N S and Nocera D G 2006 *Proc. Natl. Acad. Sci. USA* **103** 15729
[6] Lewis N S 2007 *Science* **315** 798
[7] Higashi M, Abe R, Teramura K, Takata T, Ohtani B and Domen K 2008 *Chem. Phys. Lett.* **452** 120

[8] Pinaud B A, Benck J D, Seitz L C, Forman A J, Chen Z, Deutsch T G, James B D, Baum K N, Baum G N, Ardo S, Wang E, Miller H and Jaramillo T F 2013 *Energy Environ. Sci.* **6** 1983
[9] Yang M, Oró-Sole J, Kusmartseva A, Fuertes A and Atteld J P 2010 *J. Am. Chem. Soc.* **132** 4822
[10] Fuertes A 2012 *J. Mater. Chem.* **22** 3293
[11] Page K, Stoltzfus M W, Kim Y I, Proffen T, Woodward P M, Cheetham A K and Seshadri R 2007 *Chem. Mater.* **19** 4037
[12] Zhang Y R, Masubuchi T, Masubuchi Y and Kikkawa S 2011 *J. Ceram. Soc. Jpn.* **119** 581
[13] Hinuma Y, Moriwake H, Zhang Y R, Motohashi T, Kikkawa S and Tanaka I 2012 *Chem. Mater.* **24** 4343
[14] Yang M, Oró-Solé J, Rodgers J A, Jorge A B, Fuertes A, Atteld J P 2011 *Nat. Chem.* **3** 47
[15] Tessier F and Marchand R 2003 *Journal of Solid State Chemistry* **171** 143
[16] Clarke S J, Michie C W and Rosseinsky M J 1999 *Journal of Solid State Chemistry* **146** 399
[17] Marchand R, Pors F, Laurent Y, Regreny O, Lostec J and Haussonne J M 1986 *J. Phys. Colloques.* **47** C1-901
[18] Pors F, Marchand R, Laurent Y, Bacher P and Roult G 1988 *Mater. Res. Bull.* **23** 1447
[19] Fang C M, de Wijs J A, Orhan E, de With G, de Groot R A, Hintzen H T and Marchand R J 2003 *Phys. Chem. Solids* **64** 281
[20] Perdew J P, Ruzsinszky A, Csonka G I, Vydrov O A, Scuseria G E, Constantin L A, Zhou X and Burke K. 2008 *Phys. Rev. Lett.* **100** 136406
[21] Tran F and Blaha P 2009 *Phys. Rev. Lett.* **102** 226401
[22] Blaha P, Schwarz K, Madsen G K H, Kvanicka D and Luitz J 2001 *WIEN2k, an Augmented Plane Wave plus Local Orbitals Program for Calculating Crystal Properties*, Vienna University of Technology
[23] Guo S D and Liu B G 2012 *J. Magn. Mater.* **324** 2410
[24] Zahid A, Sajad A, Iftikhar A, Imad K and Rahnamaye A 2013 *Phys. B* **420** 54
[25] Imad K, Iftikhar A, H.A. Rahnamaye A, S. Jalali A, Zahid A and Maqbool M 2013 *Comput. Mater. Sci.* **77** 145
[26] Murnaghan F D 1944 *Proc. Natl. Acad. Sci. USA* **30** 244
[27] Wolff H and Dronskowski R 2008 *J. Comput. Chem.* **29** 2260
[28] Okoye C M I 2006 *Mater. Sci. Eng. B* **130** 101
[29] Murtaza G, Ahmad I, Maqbool M, Rahnamaye Aliabad H A and Afaq A 2011 *Chin. Phys. Lett.* **28** 117801